第32卷 第9期 焊 接 学 报 Vol. 32 No. 9
2011年9月 TRANSACTIONS OF THE CHINA WELDING INSTITUTION September 2011

钛/铝异种金属搅拌摩擦焊搭接接头的组织结构

陈玉华， 倪 泉， 黄春平， 柯黎明
（南昌航空大学 轻合金加工科学与技术国防重点学科实验室，南昌 330063）

摘 要： 采用搅拌摩擦焊对TC1钛合金和LF6铝合金异种金属进行了搭接连接，研究了接头的微观组织结构. 结果表明，当搅拌头旋转频率为1 500 r/min、焊接速度为60 mm/min时，能获得焊缝成形良好、无孔洞和裂纹等缺陷的搭接接头，搭接处铝合金和钛合金充分混合，形成焊核区. 焊核两侧进入铝合金中的钛合金在搅拌针的挤压下发生了弯曲，使得钛/铝紧密结合. 搭接接头中心部位的搭接界面区呈层状组织，可分为三层，靠近焊核和靠近钛合金母材一侧的均为黑白相间的条带状组织，含有焊接过程中生成的Ti-Al金属间化合物；夹在中间的为黑色片状组织和灰色基体上分布黑色颗粒的条带状组织，分别是被搅入界面区的钛合金母材和钛合金母材与铝合金母材的机械混合物.

关键词： 钛/铝异种金属；搅拌摩擦焊；搭接接头；微观组织；元素分布
中图分类号： TG 456.9 **文献标识码：** A **文章编号：** 0253－360X(2011)09－0073－04

陈玉华

0 序 言

铝合金密度低、经济性好，钛合金在强度、耐腐蚀性等方面具有优势，随着航空发动机和飞机结构设计对“减轻重量、提高推重比、增加有效载荷”的要求越来越高，将钛合金与铝合金连接形成复合结构具有广阔的应用前景[1,2]. 赵鹏飞等人[3]对钛/铝进行了钎焊连接，研究表明在结合界面上生成层状的脆而硬的金属间化合物是钛/铝异种合金焊接所存在的主要问题. Ren等人[4]对钛和铝进行了扩散焊接，获得了无裂纹的焊接接头. 姚为等人[5]采用纯铝和纯钛为焊接材料对钛合金/铝合金进行扩散焊，结果发现接头强度取决于扩散区中冶金结合的程度及界面结构. 陈彦宾等人[6]利用散焦CO_2激光束，通过对被焊材料进行预加工坡口处理，实现了厚度为1.5 mm的Ti-6Al-4V钛合金和5056铝合金的激光熔－钎焊连接，并发现气孔是导致接头失效的主要因素.

搅拌摩擦焊是1991年发明的一种全新的固态连接方法，对克服异种材料性能差异所带来的焊接困难具有极大的优势，是比较理想的异种金属连接方法. 目前国内外关于钛/铝异种金属搅拌摩擦焊的研究极少，Dressler等人[7]用搅拌摩擦焊技术实现了Ti-6Al-4V钛合金和2024-T3铝合金的对接焊，焊接接头的抗拉强度达到铝合金母材的73%. Chen等人[8]采用搅拌摩擦焊技术对纯钛和Al-Si合金进行了搭接连接，观察了接头的微观组织、相结构，测试了接头的性能.

采用搅拌摩擦焊方法对TC1钛合金和LF6铝合金异种金属进行了搭接连接，研究了接头的显微组织和元素分布，为进一步改进工艺、获得优质焊接接头、促进钛/铝异种金属搅拌摩擦焊结构的应用奠定基础.

1 试验方法

试验材料为LF6铝合金和TC1钛合金，厚度为2 mm，其化学成分和力学性能如表1、表2所示.

表1 LF6铝合金的化学成分和力学性能

Table 1 Composition and mechanical property of LF6

化学成分(质量分数，%)							抗拉强度	断后伸长率
Mn	Mg	Si	Cu	Fe	Zn	Al	R_m/MPa	A(%)
0.6	5.8	0.3	0.1	0.3	0.15	余量	320	15

焊接时，钛合金和铝合金的相对位置按图1所示. 试验采用的搅拌头用高温合金制成，搅拌头轴

收稿日期： 2010－08－02
基金项目： 航空科学基金资助项目(2009ZE56011)；轻合金加工科学与技术国防重点学科实验室开放基金资助项目(gf200901001)

表 2 TC1 钛合金的化学成分和力学性能

Table 2 Composition and mechanical property of TC1

化学成分(质量分数,%)								抗拉强度 R_m/MPa	断后伸长率 A(%)
Al	Mn	Fe	Si	C	O	N	Ti		
2.0	1.8	0.1	0.15	0.1	0.15	0.05	余量	650	20

肩直径为 13 mm,搅拌针直径为 5 mm,表面加工有右螺纹. 用自制的焊接夹具在铣床改装的搅拌摩擦焊机上进行焊接试验,在大量预试验的基础上选取搅拌头的旋转频率为 1 500 r/min、焊接速度为 60 mm/min,搅拌头倾角为 2°.

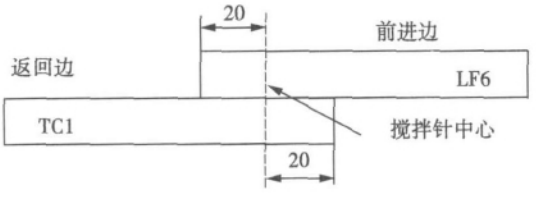

图 1 钛合金与铝合金相对位置示意图(mm)

Fig. 1 Sketch of relative position between Ti alloy and Al alloy

焊后沿垂直于焊缝横截面方向制备金相试样,采用 Kroll 试剂(2 mLHF + 4 mLHNO_3 + 94 mLH_2O)对铝合金一侧接头进行侵蚀,采用 NaOH 水溶液(2 gNaOH + 100 mLH_2O)对钛合金一侧接头进行侵蚀,在 4XB-TV 倒置金相显微镜上配合 Leica 图像分析仪观察焊缝表面、横截面宏观形貌和接头金相组织,采用 Quanta 200 型扫描电镜观察界面区的微观组织结构,采用能谱仪分析焊接接头的元素分布和含量,用 HVS-1000 型数显显微硬度计测量焊接接头的显微硬度分布,加载载荷为 1.96 N.

2 结果与分析

2.1 搭接接头表面及横截面形貌

焊接接头表面和横截面的宏观形貌如图 2 所示. 由图 2a 可知,在所选的工艺参数下,焊缝表面光滑、弧形纹致密而均匀,无沟槽和裂纹等缺陷.

由图 2b 可见,钛合金被搅进了铝合金之中,搭接处铝合金和钛合金充分混合,形成了焊核区,且焊核两侧的钛合金在铝合金母材形成了形似弯钩状的分布,使得两者结合紧密,整个焊接接头横截面成形良好,无孔洞、裂纹等缺陷. 因此,采用搅拌摩擦焊技术在所选用的工艺参数下能获得成形良好的钛合金/铝合金异种金属搭接接头.

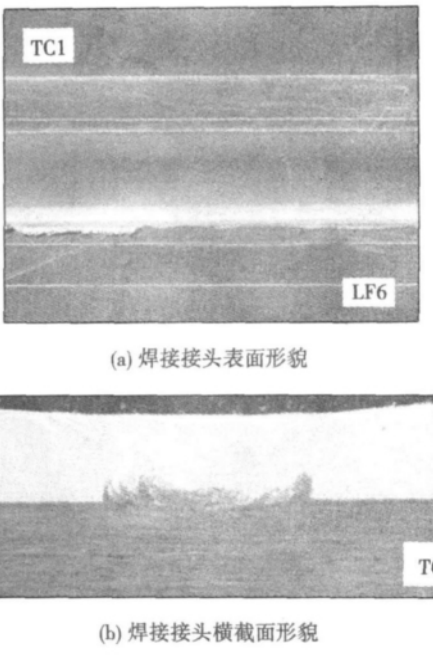

(a) 焊接接头表面形貌

(b) 焊接接头横截面形貌

图 2 钛/铝搭接接头的宏观形貌

Fig. 2 Macro-profile of lap joint of Ti/Al

2.2 焊接接头的微观组织

图 3 为焊接接头的金相组织,LF6 铝合金母材为轧制的条状组织(图 3a),TC1 钛合金母材的组织为($\alpha+\beta$)相(图 3b). 在搭接界面处,钛合金、铝合金发生了较大程度的混合,形成了既不同于铝合金母材组织也不同于钛合金母材组织的混合区(图 3c). 在高倍下观察焊核区的边侧部位(图 3c 中的 M 区)和中心部位(图 3c 中的 N 区)的微观组织结构,分别如图 3d 和图 3e 所示. 由图 3d 可见,焊核两侧进入铝合金的钛合金在搅拌针的挤压下发生了弯曲,呈“弯钩状”或“钳状”,使得钛合金和铝合金紧密结合. 被搅入焊核的钛合金中也混入了少量的铝合金. 由图 3e 可见,该处的钛合金已达到了塑性状态,并且在搅拌头的搅拌和挤压作用下发生了流动,使部分钛合金进入了铝合金中,两种材料呈交迭分布.

分析其原因是焊核区塑化金属在搅拌针螺纹的摩擦力和压力共同作用下,向上作螺旋形运动,迫使焊核周围塑化的钛合金金属进入铝合金中,而同时又受到轴肩处金属的挤压和焊缝下部出现的瞬时低压作用,呈向下运动趋势,因此最终呈现出钛合金以“弯钩状”或“钳状”形式和铝合金紧密结合,钛合金和铝合金呈交迭分布.

2.3 界面区微观结构及元素含量

采用扫描电镜和能谱分析仪对搭接界面区中心部位(图 3c 中的 N 区)的微观结构和成分进行进一步分析,如图4所示. 从图4可以看出,TC1钛合金

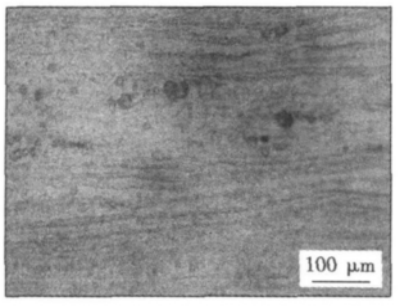

(a) LF6铝合金母材显微组织

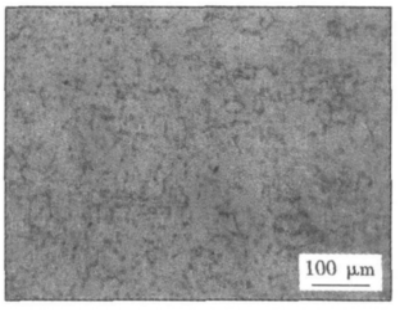

(b) TC1钛合金母材显微组织

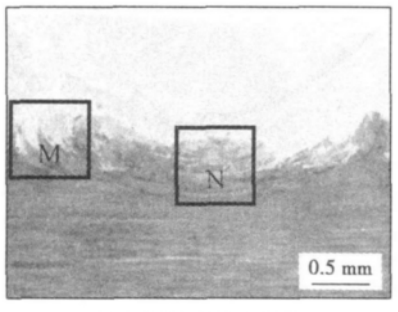

(c) 界面区的显微组织

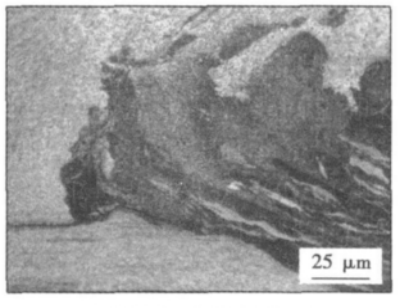

(d) 图3c中M区的局部放大

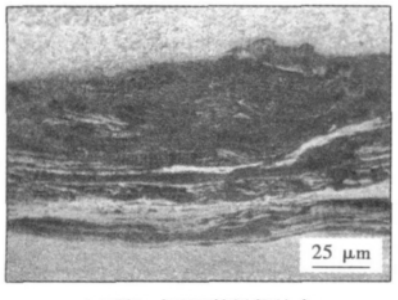

(e) 图3c中N区的局部放大

图 3　钛/铝搭接接头的微观组织

Fig. 3　Microstructure of Ti/Al lap joint

/LF6 铝合金搅拌摩擦焊搭接接头的搭接界面区呈层状组织，可分为三层（图 4 中区域 1、区域 2、区域 3），靠近焊核和靠近钛合金母材一侧的均为黑白相间的组织（图 4 中区域 3），区域 1 为黑色条状组织，区域 2 为灰色基体上分布着黑色的颗粒.

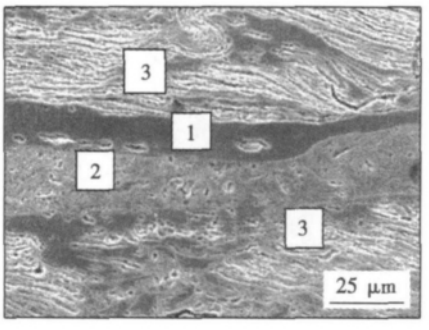

图 4　搭接界面区的扫描电镜形貌

Fig. 4　SEM morphology of interfacial zone

对区域 1、区域 2、区域 3 分别进行能谱分析，测试其元素种类和含量，结果如图 5 和表 3 所示，可以看出，区域 1 的元素种类和含量与 TC1 钛合金母材基本接近，因此是被搅入了界面区的条状TC1钛合

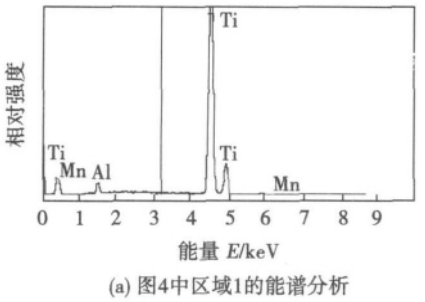

(a) 图4中区域1的能谱分析

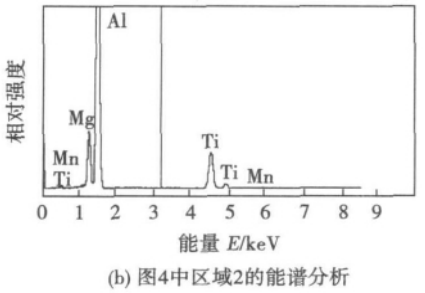

(b) 图4中区域2的能谱分析

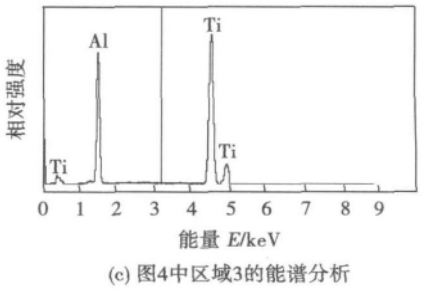

(c) 图4中区域3的能谱分析

图 5　搭接界面区能谱分析结果

Fig. 5　Energy spectrum analysis of interfacial zone

表 3 搭接界面区各层元素的含量(原子分数,%)

Table 3 Chemical composition of interfacial zone

区域	Ti	Al	Mg	Mn
1	95.09	4.00	—	0.91
2	10.79	78.60	10.17	0.44
3	58.91	41.09	—	—

金母材; 区域 2 中以 Al 元素为主,但含有一定数量的 Ti 和 Mg 元素,因此是 TC1 钛合金母材和 LF6 铝合金母材的机械混合物; 区域 3 中只含有 Ti 和 Al 两种元素,且其原子比接近 1∶1,因此钛合金母材和铝合金母材在搅拌头的摩擦、挤压作用下该区可能形成了 Ti-Al 金属间化合物.

3 结 论

(1) 采用搅拌摩擦焊对钛合金/铝合金进行搭接焊接时,当搅拌头的旋转频率为 1 500 r/min、焊接速度为 60 mm/min 时,能获得良好的焊缝成形,焊缝表面光滑、弧形纹致密而均匀,搭接处铝合金和钛合金充分混合,形成焊核区,焊接接头无孔洞、裂纹等缺陷.

(2) 焊核两侧进入铝合金中的钛合金在搅拌针的挤压下发生了弯曲,呈"弯钩状"或"钳状",使得钛合金和铝合金紧密结合. 被搅入焊核的钛合金中也混入了少量的铝合金.

(3) 搭接接头中心部位的搭接界面区呈层状组织,可分为三层: 靠近焊核和靠近钛合金母材一侧的均为黑白相间的条带状组织,夹在中间的为黑色条状组织和灰色基体上分布黑色颗粒的条带状组织. 黑白相间的条带状组织含有焊接过程中生成的 Ti-Al 金属间化合物; 黑色条状组织是被搅入界面区的 TC1 钛合金母材,灰色基体上分布黑色颗粒的条带状组织是 TC1 钛合金母材和 LF6 铝合金母材的机械混合物.

参考文献:

[1] Sohn H W, Bong H H, Hong S H. Microstructure and bonding mechanism of Al/Ti Bonded joint using Al-10Si-1Mg filler metal [J]. Materials Science and Engineering A, 2003(355): 231 - 240.

[2] Ren Jianwei, Li Yajiang, Feng Tao. Microstructure characteristics in the interface zone of Ti/Al diffusion bonding [J]. Materials Letters, 2002, 56(5): 647 - 652.

[3] 赵鹏飞, 康 慧. Al-Ti 异种合金真空钎焊的研究 [J]. 材料工程, 2001(4): 25 - 28.
Zhao Pengfei, Kang Hui. Study on vacuum brazing of dissimilar alloys of Al/Ti [J]. Journal of Materials Engineering, 2001(4): 25 - 28.

[4] Wilden J, Bergmann J P. Manufacturing of titanium/aluminum and titanium/steel joints by means of diffusion welding [J]. Welding and Cutting, 2004, 3(5): 285 - 290.

[5] 姚 为, 吴爱萍, 邹贵生, 等. Ti/Al 扩散焊的接头组织结构及其形成规律 [J]. 稀有金属材料与工程, 2007, 36(4): 700 - 704.
Yao Wei, Wu Aiping, Zou Guisheng, *et al*. Structure and forming process of the Ti/Al diffusion bonding joints [J]. Rare Metal Materials and Engineering, 2007, 36(4): 700 - 704.

[6] 陈树海, 李俐群, 陈彦宾. Ti/Al 异种合金激光焊熔钎焊过程气孔形成机制 [J]. 稀有金属材料与工程, 2010, 39(1): 32 - 36.
Chen Shuhai, Li Liqun, Chen Yanbin. Formation mechanism of porosity in laser welding-brazing of Ti/Al dissimilar alloys [J]. Rare Metal Materials and Engineering, 2010, 39(1): 32 - 36.

[7] Ulrike Dressler, Gerhard Biallas, Ulises Alfaro Mercado. Friction stir welding of titanium alloy TiAl6V4 to aluminium alloy AA2024-T3 [J]. Materials Science and Engineering A, 2009, 526(1 - 2): 113 - 117.

[8] Chen Y C, Nakata K. Microstructural characterization and mechanical properties in friction stir welding of aluminum and titanium dissimilar alloys [J]. Materials and Design, 2009(30): 469 - 474.

作者简介: 陈玉华,男,1979 年出生,博士,副教授,硕士生导师. 主要从事先进材料及其连接技术方面的科研和教学工作. 发表论文 40 余篇. Email: ch.yu.hu@163.com

arc length control; pulsed MIG welding

Effect of current field on Ti/TiAl interface and mechanical performance LIU Zefeng, CHEN Shaoping, LIANG Lianjie, MENG Qingsen (Department of Material Science and Engineering, Taiyuan University of Technology, Taiyuan 030024, China). p 57 – 60

Abstract: Ti /TiAl gradient materials were prepared by field-activated pressure-assisted synthesis (FAPAS) process. The microstructure, phase composition and fracture morphography of the interface were analyzed by SEM and XRD. The bending strength of the sample was tested by three-point bending test. Meanwhile, finite element analysis with ANSYS code was used to calculate the mechanical properties such as residual stress and deformation. It was shown that fine TiAl particles were formed with FAPAS and maximum bending strength as high as 346 MPa was obtained in the Ti/TiAl interface. The interface were layered gradient structure of $TiAl/Ti_3Al/Ti$ (ss. Al) /Ti. The fracture located in the TiAl–Ti_3Al interface, and showed brittle fracture morphology. The maximum residual stress sited in the TiAl–Ti_3Al interface, which was the position of weakness of the material.

Key words: field-activated; finite element analysis; diffusion bonding; residual stress

Microstructure analysis of fusion layer melted CrFeNb on Ni-base superalloy AI Changhui[1], ZHAO Zhilong[1], SU Jian[1], LI Jingwei[2] (1. School of Mechatronics, Northwestern Polytechnical University, Xi´an 710072, China; 2. Engineering Training Center, Northwestern Polytechnical University, Xi´an 710100, China). p 61 – 64

Abstract: A coating has been made on K4169 substrate by argon arc cladding technique with the inter-metallic compound (IMC) of CrFeNb. The microstructure and element distribution of the cladding coating were analyzed by scanning electron microscope (SEM) and energy-dispersive spectrum (EDS). The results showed that a fusion layer with a thickness of 64.8 μm was formed between the K4169 substrate and CrFeNb. In the fusion layer, the dendritic solidification of cladding CrFeNb stretched into the substrate and cross joined, which formed favorable metallurgical conjunction without the metallurgical defects such as alveolate air holes or cracks. According to the proportion relationship of atomic numbers, two new composite phases of Cr–Fe–Ni–Nb were formed in the fusion layer, and the calculated results showed that they were $Cr_{(7.16\sim25.0)}$–$Fe_{(6.39\sim23.4)}$–$Ni_{(10.6\sim56.9)}$–Nb and $Cr_{(1.60\sim3.48)}$–$Fe_{(1.44\sim3.11)}$–$Ni_{(2.84\sim7.20)}$–Nb, respectively.

Key words: argon arc; inter-metallic compounds; fusion layer; solidification

Microstructure and mechanical properties of ZrO_2 ceramic and kovar brazed joints LIN Xiaochao, CAO Jian, ZHANG Lixia, Feng Jicai (Key Laboratory for Advanced Welding Droduction Technology, Harbin Institute of Technology, Harbin 150001, China). p 65 – 68

Abstract: Brazing of ZrO_2 ceramic to Kovar alloy was successfully realized by using self-developed Ag-Cu-TiH_2 filler powder at the 825 ~ 960 ℃ for 1 ~ 60 min. Interface microstructures were investigated by scanning electron microscopy, X-ray diffraction and EDS energy spectrum. The results showed that the typical interface microstructure of brazed joints from Kovar side to ZrO_2 ceramic side could be expressed as Kovar/Ag(s. s) + Cu(s. s) + $TiFe_2/TiNi_3$ + $TiFe_2$ + Ti–Fe–Ni/Ag(s. s) + Cu(s. s) + $TiFe_2/Cu_2Ti_4O$/TiO + Zr_xO_y/ZrO_2. The maximum shear strength of the joints was 134 MPa, which was achieved when the brazing temperature was 875 ℃ and holding time was 10 min. The brittle fracture took place on the TiC interface. When the brazing temperature and holding time changed, the brazed joints weakened and the shear strength decreased.

Key words: ZrO_2 ceramic; Kovar alloy; brazing; interfacial microstructure; shear strength

Effect of micro B on wettability of Cu-P based quenching filler metals ZOU Jiasheng, XU Xiangping, WANG Lei (Provincial Key Lab of Advanced Welding Technology, Jiangsu University of Science and Technology, Zhenjiang 212003, China). p 69 – 72

Abstract: Three different components of the Cu-P based filler metal foils were prepared by single-roll rapidly-cooled equipment. The melting feature and structure were analyzed with DTA and XRD methods. The wettability of Cu-P based filler metals on copper was studied. The results showed that, compared with the conventional filler metals, the quenching filler metals had lower melting temperature and narrower melting temperature range. The quenching filler metal containing 0.03% B had the lowest liquidus temperature and the narrowest melting temperature range. The structures of the quenching filler metals with 0.03wt% B and 0.04% B were amorphous. In the same process conditions, the quenching filler metal contained 0.03wt% B had best wettability on copper. As with brazing temperature and time increased, the wettability of Cu-P based quenching filler metal appears increased first and then decreased. Compared with conventional brazing filler metals , the wettability of quenching filler metal has been improved significantly.

Key words: Cu-P based filler metal; quenching; amorphous filler metal; wettability

Microstructure of Ti/Al dissimilar alloys lap joint made by friction stir welding CHEN Yuhua, NI Quan, HUANG Chunping, KE Liming (National Defense Key Disciplines Laboratory of Light Alloy Processing Science and Technology, Nanchang Hangkong University, Nanchang 330063, China). p 73 – 76

Abstract: Dissimilar metals of TC1/LF6 were lap jointed by friction stir welding (FSW) and the microstructure of the lap joint was studied. The results showed that good appearance of weld joint without defects such as cavitation and crack was obtained when the rotation speed of stir head was 1 500 r/min and the welding speed was 60 mm/min. Ti alloy and Al alloy intensively mix and form nugget zone in the lap zone. Ti alloy which is stirred into Al alloy on both sides of the nugget bends under the extrusion effection of the pin and tight couples with Al alloy. The microstrucrure in the interfacial zone of the lap joint center is lamellarstructure and can be divided into three layers. The layer closed to the nugget zone and TC1 base metal is black and white stripped structure which contains Ti–Al intermetallic compound generated during FSW. The layers in the center are black lamellar structure and stripped structure with black particles distributing on the gray matrix. Black lamellar structure is TC1 base metal which is stirred into the interfacial zone, and the stripped structure with black particles distributing on the gray matrix is

mechanical mixture of TC1 base metal and LF6 base metal.

Key words: dissimilar matals of Ti/Al; friction stir welding; lap joint; microstrcture; element distribution

Comparision of corrosion properties for 5083 aluminum alloy friction stir welding and metal inert-gas welding weld

ZHAO Yadong[1], WANG Zhigang[1], SHEN Changbin[2], GE Jiping[2], Huang Zhenhui[3] (1. School of Mechanical Engineering, Anyang Institute of Technology, Anyang 455000, China; 2. School of Materials Science and Engineering, Dalian Jiaotong University, Dalian 116028, China; 3. R&D Center, CNR Tangshan Railway Vehicle Co., Ltd, Tangshan 063035, China). p 77 - 80

Abstract: The microstructures and corrosion properties of 5083 aluminum alloy friction stir welding (FSW) and MIG (metal inert-gas) weld were analyzed. The results showed that the FSW weld was characterized by its much finer grains, contrasting with the grains of MIG weld. Electrochemical corrosion test demonstrated that the corrosion potential of the FSW weld at the rotation rate of 300 r/min, and the traverse speed of 160 mm/min with 3° tool tilt was more positive than that of the MIG weld, meanwhile, the corrosion rate and the corrosion current density were less than those of the MIG weld, Rp (polarization resistance) of the FSW weld was larger than that of the MIG weld. The corrosion morphologies analysis showed that few shallow pits presented on the surface of the dissimilar weld. However, a large number of deeper pits emerged on the surfaces of two parent materials.

Key words: 5083 aluminum alloy; friction stir welding (FSW); metal inert-gas welding (MIG); weld; corrosion properties

Microstrucutre analysis of superplastic deformation on laser butt weld Ti-6Al-4V joint

CHENG Donghai, CHEN Yiping, HU Dean, WEI Qiang (School of Aeronautical Manufacturing Engineering, Nanchang Hangkong University, Nanchang 330063, China). p 81 - 84

Abstract: Microstructures of welded joints before and after superplastic deformation were observed by optical microscope, and the forming mechanism was discussed. The results indicated that increasing temperature and decreasing velocity were good for superplastic deformation, and the grains of base metal grew coarser and the phase ratio increased. Needle-like martensite phase of weld bead became shorter and wider, exhibiting globing trend under higher temperature. The maximal microhardness of cross section of weld bead after deformation is 380 HV, about 50 HV lower compares with original weld bead, which meets the requirnement of the actucal lead.

Key words: titanium alloy; welding/superplastic deformation; mirostructure

Microstructure and mechanical property of dissimilar material resistance spot welded joint of steel and aluminum alloy with electrode plate

ZHANG Weihua[1], SUN Daqian[1], LI Zhidong[2], LIU Dongyang[1], LI Dandan[1] (1. Key Laboratory of Automobile Materials, School of Materials Science and Engineering, Jilin University, Changchun 130022, China; 2. Engineering Training Center, Jilin University, Changchun 130022, China). p 85 - 88

Abstract: Dissimilar materials of H220YD high strength steel and 6008-T66 aluminum alloy had been joined by resistance spot welding with electrode plate. Microstructure and mechanical property of the dissimilar material welded joint were investigated. The results indicated that the welded joint was achieved by means of wetting and spreading of liquid aluminum alloy on solid steel surface, hence it could be regarded as a special welded-brazed joint. A thin dual-layered intermetallic compound layer composed of Fe_2Al_5 and $FeAl_3$ was formed on the steel/aluminum alloy interface. The diameter of aluminum alloy nugget of the welded joint reached the maximum value of 9.5 mm at welding speed of 14 kA and welding time of 300 ms. With the increase of welding current (8-14 kA), the tensile-shear load of the welded joint increased rapidly first (8-12 kA) and then became calm gradually (12-14 kA). The tensile-shear load was up to 4.3 kN at welding current of 12 kA and welding time of 300 ms, which was about 30% higher than that of the welded joint obtained without electrode plate. During tensile shear testing, the cracking developed through the brittle intermetallic compound layer and partially in the aluminum alloy nugget.

Key words: high strength steel; aluminum alloy; resistance spot welding; electrode plate

Investigation on penetration of pulsed twin deposition electrode arc welding

JIAN Mingjian, ZOU Zengda, WANG Yufu (Key Laboratory for Liquid-Solid Structural Evolution & Processing of Materials Ministry of Education, Shandong University, Jinan 250061, China). p 89 - 92

Abstract: Effects of pulsed parameters on weld penetration with the method of orthogonal experiment were researched when pulse power supply was applied to twin deposition electrode arc welding. Results of orthogonal experiment indicated the change of pulsed parameters could result in the corresponding change of weld penetration, and the descending order of pulsed parameters influencing weld penetration was as follows: peak current > frequency > duty ratio > base current. Greater penetration could be obtained with these pulsed parameters: peak current of 230-240 A, frequency of 3.3-3.7 Hz, duty ratio of 48%-52% and base current of 160-175 A. Optimal combination of pulse parameters of obtaining greater penetration is determined, which is frequency of 3.5 Hz, peak current of 230 A, base current of 160 A and duty ratio of 50%. Weld penetration increases when pulse power supply is applied to twin deposition electrode arc welding.

Key words: pulsed parameters; orthogonal experiment; weld penetration

Effect of processing parameters on microstructure and mechanical properties of pure copper joints made by friction stir welding

LI Xiawei, ZHANG Datong, QIU Cheng, ZHANG Wen (State Engineering Research Center for Metallic Materials Net-shape Processing, South China University of Technology, Guangzhou 510640, China). p 93 - 96

Abstract: The main objective of this investigation was to apply friction stir welding (FSW) for joining of pure copper plate which is 3 mm thick. Defect free welds were obtained at a constant rotation speed of 800 r/min and travel speed ranging from 60 mm/min to 300 mm/min. The influence of welding parameters on the microstructure and mechanical properties of the pure copper joints were investigated. The joints exhibit four distinct zones, parent material, heat affect zone, thermo-mechanically